Spatially modulated thermal convection of viscoelastic fluids

Séliatou Kayodé
Laboratoire de Mécanique et Matériaux 1, Ecole Centrale de Nantes, rue de la Noë, Boîte Postale 62116, 44321 Nantes Cedex 03, France

Roger E. Khayat*
Department of Mechanical and Materials Engineering, University of Western Ontario, London, Ontario, Canada N6A 5B9
(Received 4 December 2003; published 24 June 2004)

The thermal convection of modulated viscoelastic flow is examined in this study. The modulation is assumed to be weak enough for a regular perturbation solution to be implemented. In addition to being more accurate, the second-order perturbation results reveal new physical phenomena that could not be predicted by the first-order analysis. Inertia was found to enhance globally the discrepancies between the first- and the second-order perturbation solution. A comparison between the Newtonian and the non-Newtonian solution is carried out and the influences of inertia, modulation amplitude, and wave number are emphasized. The present results show that elasticity has a marked effect on fluid patterns, especially regarding the roll structure and symmetry. The influence of elasticity is greater for larger Rayleigh number and aspect ratio.

DOI: 10.1103/PhysRevE.69.066319 PACS number(s): 47.20.Bp, 47.20.Ky

I. INTRODUCTION

Thermal convection and flow in a microchannel with modulated walls is a classical problem that has attracted renewed interest because of its immediate relevance to novel microtechnologies, such as compact heat exchangers, and membrane blood oxygenators in extracorporeal systems [1]. Moreover, the analysis of such flows can help to understand the generation of wind waves due to the change in the surface of the earth temperature as well as the atmosphere [2]. The flow can exhibit many of the features present in much more complex geometries, which can significantly impact heat or mass transfer performance. This richness in physical phenomena in a relatively simple geometry motivates fundamental interest by providing an ideal setting to understand pattern formation for both Newtonian and non-Newtonian fluids [3].

The effects of spatial wall variations on the steady flow between smooth boundaries were examined only relatively recently [see Ref. [4] and bibliography therein]. One may refer to such variations from perfect geometries as dirty effects. On the other hand [5], these deviations can lead to interesting phenomena, which are not present in systems of high geometry. Sidewalls, for example, may restrict the structure of stable wave numbers for cellular patterns or modify the orientation of convection rolls [6–8]. Reflection effects [9] or dynamical structures [10] can be induced in systems such as rotating Rayleigh-Bénard convection. Irregularities at the boundaries may lead to localized cellular structures at the threshold of convection, similar to those of gravity waves [11]. Such phenomena modify the bifurcation behavior of cellular structures, as shown for a model system [12].

To gain insight on the effects of roughness in pattern formation, it is often helpful to have it replaced with periodic modulations. One may replace, for instance, imperfections at the boundaries in convection by temperature variations and analyze their consequences for the onset of convection. Davis [13] studied the case of temporal periodic variations. Kelly and Pal [14] examined the effects of spatially periodic boundary conditions on the stability of the Rayleigh-Bénard problem. Chen and Whitehead [15] evaluated the extent to which well-defined initial perturbations affect stable boundaries, although they were steady in time. The practical value is that one might want to make the boundary wavy if the mean Nusselt number could be increased, which have motivated Watson and Poots [16] to study the effects of wavy boundaries on laminar free convection in a flow between parallel vertical walls.

Other modulated systems have also been examined, such as the flow through sinusoidally shaped channels. Steady flow [4,17], as well as stability aspects were considered [18,19]. Modulated rotating flow was also considered. Recently, Li and Khayat showed the existence of interesting pattern formation in modulated Taylor-Couette flow for Newtonian fluids [20].

Interesting effects in pattern formation are related to finite size or inhomogeneity effects. However, the flow of complex fluids present additional exciting phenomena. In the present paper, the modulated thermal convection of viscoelastic fluids is examined. The solution is obtained by mapping the physical domain onto the rectangular computation domain, and applying a perturbation representation for the transformed equations, similarly to Zhou *et al.* [4,17]. The results based on the perturbation method will be benchmarked against results obtained from a traditional finite-volume formulation for Newtonian thermal convection. The influence of the Rayleigh number, Deborah number, dimensionless wave number, and amplitude on the flow and heat transfer is emphasized.

*Corresponding author. Email address: rkhayat@eng.uwo.ca

II. PROBLEM FORMULATION AND SOLUTION PROCEDURE

In this section, the general equations and boundary conditions for the steady-state flow of a viscoelastic fluid in a weakly modulated channel are derived for a small-amplitude modulation. A regular perturbation expansion for the flow field is carried out after the equations are mapped over a rectangular domain, reducing the problem to a set of ordinary differential equations with homogeneous boundary conditions, which will be solved using a variable-step-finite-difference scheme.

A. Governing equations and boundary conditions

Consider the steady-state flow of an incompressible non-Newtonian fluid lying horizontally between two infinite rigid stationary boundaries, the lower being straight and the upper periodically modulated. Let T_0 and $T_0+\delta T$ be the temperatures of the upper and lower plates, respectively, with δT being the temperature difference. The problem is first introduced in the (X,Z) plane, with the X axis taken along the lower wall and the Z axis along the direction perpendicular to the plates. The general shapes of the lower and upper plates are given by $Z=0$ and $D+Af(X)$, respectively. D is the mean channel width and A is the modulation amplitude. Here $f(X)$ is a general dimensionless function of X that may be arbitrarily prescribed. In this work, however, a sinusoidal modulation will be considered. The substances of main interest are assumed to obey the following equation of state:

$$\rho = \rho_0[1-\beta(T-T_0)], \tag{1}$$

where ρ_0 is the density at T_0 and β is the coefficient of volumetric expansion.

The fluid is assumed to be incompressible viscoelastic polymeric solution of density ρ, relaxation time λ, and viscosity μ. In this study, only fluids that can be reasonably represented by a single relaxation time and constant viscosity are considered. The polymeric solution is assumed to be composed of a Newtonian solvent of viscosity μ_s, and a polymeric solute of viscosity μ_p, such that the solution viscosity is given by $\mu=\mu_s+\mu_p$. Regardless of the nature of the fluid, the continuity and momentum balance equations must hold. If the Boussinesq approximation, which states that the effect of compressibility is negligible everywhere in the conservation equations except in the buoyancy term, is assumed to hold, then, the equations for conservation of mass, momentum, and energy read, respectively,

$$\boldsymbol{\nabla}\cdot\mathbf{U}=0, \tag{2}$$

$$\rho_0\mathbf{U}\cdot\boldsymbol{\nabla}\mathbf{U}=\boldsymbol{\nabla}\cdot\boldsymbol{\sigma}+\rho\mathbf{g}, \tag{3}$$

$$\mathbf{U}\cdot\boldsymbol{\nabla}T=\kappa\boldsymbol{\nabla}^2T, \tag{4}$$

where $\mathbf{U}(U,W)$ is the velocity vector, $\boldsymbol{\sigma}$ is the stress tensor, $\boldsymbol{\nabla}$ is the two-dimensional gradient operator, $\mathbf{g}$ is the gravity acceleration vector, κ is the thermal diffusivity, and T is the temperature. The deviatoric part of the stress tensor $\boldsymbol{\sigma}$ is composed of a Newtonian component, corresponding to the Newtonian solvent, and a polymeric component $\mathbf{T}$ corresponding to the solute. Thus,

$$\boldsymbol{\sigma}=-P\mathbf{I}+\mu_s(\boldsymbol{\nabla}\mathbf{U}+\boldsymbol{\nabla}\mathbf{U}^t)+\mathbf{T}, \tag{5}$$

where P is the hydrostatic pressure, $\mathbf{I}$ is the identity matrix, and t denotes matrix transposition. The constitutive equation for $\mathbf{T}$ is taken to correspond to an Oldroyd-B fluid, which can be written as [21]

$$\lambda(\mathbf{U}\cdot\boldsymbol{\nabla}\mathbf{T}-\mathbf{T}\cdot\boldsymbol{\nabla}\mathbf{U}-\boldsymbol{\nabla}\mathbf{U}^t\cdot\mathbf{T})+\mathbf{T}=\mu_p(\boldsymbol{\nabla}\mathbf{U}+\boldsymbol{\nabla}\mathbf{U}^t). \tag{6}$$

In the limit $\mu_s\to 0$, the system (1)–(6) reduces to that corresponding to a Maxwell fluid. On the other hand, in the limit $\mu_p\to 0$, the Newtonian fluid is recovered. The boundary conditions are given by

$$\mathbf{U}(X,Z=0)=\mathbf{U}(X,Z=D+Af)=\mathbf{0},$$

$$T(X,Z=0)=T_0+\delta T,$$

$$T(X,Z=D+Af)=T_0. \tag{7}$$

The dimensionless coordinates, x and z, velocity components u and w, pressure and components of $\mathbf{T}$ p, q, r, and s, and temperature θ are introduced as follows:

$$x=\frac{X}{D},\quad z=\frac{Z}{D},\quad u=\frac{DU}{\kappa},\quad \theta=\frac{T-T_0}{\delta T},$$

$$p=\frac{D^2}{\mu\kappa}(P+\rho_0 gZ),\quad (q,r,s)=\frac{D^2(T_{zz},T_{xx},T_{xz})}{\mu\kappa}. \tag{8}$$

Five dimensionless groups emerge in the problem, namely, the Rayleigh number, the Prandtl number, the Deborah number, the solvent-to-solute ratio R_V, and the aspect ratio ε:

$$\mathrm{Ra}=\frac{\delta T g\beta D^3}{\kappa\nu},\quad \mathrm{Pr}=\frac{\nu}{\kappa},\quad \mathrm{De}=\frac{\kappa\lambda}{D^2},\quad \mathrm{Rv}=\frac{\mu_s}{\mu_p},\quad \varepsilon=\frac{A}{D}, \tag{9}$$

where $\nu=\mu/\rho$, is the kinematic viscosity. In this case, the equations for conservation of mass, momentum, and energy become

$$u_x+w_z=0, \tag{10}$$

$$\mathrm{Pr}^{-1}(uu_x+wu_z)=-p_x+aR\mathrm{v}\Delta u-r_x-s_z, \tag{11}$$

$$\mathrm{Pr}^{-1}(uw_x+ww_z)=-p_z+aR\mathrm{v}\Delta w+\mathrm{Ra}\,\theta-s_x+q_z, \tag{12}$$

$$u\theta_x+w\theta_z=\Delta\theta, \tag{13}$$

whereas the constitutive equation (6) leads to

$$us_x+ws_z-(u_zq+w_xr)=-\mathrm{De}^{-1}[s+a(u_z+w_x)], \tag{14}$$

$$ur_x+wr_z-2(u_zs+u_xr)=-\mathrm{De}^{-1}(r+2a\,u_x), \tag{15}$$

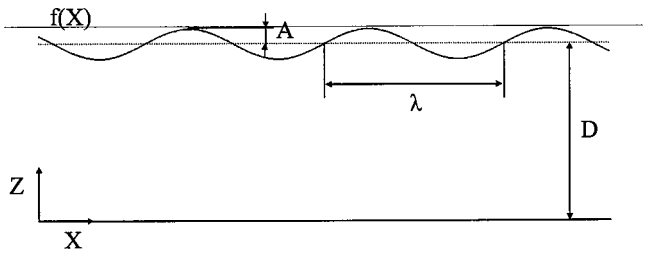

FIG. 1. Physical domain and flow configuration for a spatially modulated channel.

$$uq_x + wq_z - 2(w_z q + w_x s) = -\mathrm{De}^{-1}(q + 2a\, w_z), \quad (16)$$

where a subscript denotes partial differentiation, Δ is the two-dimensional Laplacian operator, and $a=1(R_v+1)=\mu_p/\mu$ is the polymer-to-solution viscosity ratio. The above equations must be solved subject to the following boundary conditions:

$$u(x,z=0) = u(x,z=1+\varepsilon f) = w(x,z=0) = w(x,z=1+\varepsilon f) = 0,$$

$$\theta(x,z=0) = 1, \quad \theta(x,z=1+\varepsilon f) = 0. \quad (17)$$

It is further assumed that the flow field (velocity and pressure) is spatially periodic, commensurately with the wall modulation. This periodicity condition is written as

$$u(x=0,z) = u(x=2\pi/\alpha,z), w(x=0,z) = w(x=2\pi/\alpha,z),$$

$$\theta(x=0,z) = \theta(x=2\pi/\alpha,z), p(x=0,z) = p(x=2\pi/\alpha,z),$$

$$q(x=0,z) = q(x=2\pi/\alpha,z), r(x=0,z) = r(x=2\pi/\alpha,z),$$

$$s(x=0,z) = s(x=2\pi/\alpha,z), \quad (18)$$

where α is the dimensionless channel wave number related to the wavelength λ by the relation: $\lambda=2\pi/\alpha$. The problem (11)–(19) is defined over the physical domain $\Omega_{xz}=\{(x,z)/x\in[0,\lambda];z\in[0,1+\varepsilon f(x)]\}$, which is next mapped onto the rectangular domain. The physical domain and flow configuration are schematically illustrated in Fig. 1.

B. Domain transformation

The periodic physical domain Ω_{xz} is mapped onto the rectangular domain $\Omega_{\xi\eta}=\{(\xi,\eta)/\xi\in[0,\lambda];\eta\in[0,1]\}$. Here,

$$\xi(x,z) = x, \eta(x,z) = \frac{z}{1+\varepsilon f(x)}, \quad (19)$$

where $1+\varepsilon f(x)$ is the dimensionless gap. The transformed equations and boundary conditions are given in Appendix A. The solution to Eqs. (A1)–(A7) is sought subject to conditions (A8). This is a difficult nonlinear two-dimensional problem, with variable coefficients in the governing equations. There are, however, some limit flows that may be considered, which can simultaneously be of practical and fundamental significance.

C. Perturbation expansion and solution procedure

In this work, only small-amplitude modulation is examined, so that ε is small ($\varepsilon\ll 1$). A regular perturbation expansion is used on the velocity, the pressure, the temperature, and the stress components:

$$\mathbf{v}=\mathbf{v}^0 + \varepsilon\mathbf{v}^1 + \varepsilon^2\mathbf{v}^2 + O(\varepsilon^3), \quad (20)$$

where $\mathbf{v}=(u,e,\theta,p,q,r,s)$. Terms of $O(\varepsilon^3)$ and higher are neglected. Substitution of expressions (20) into Eqs. (A1)–(A7) and conditions (A8) leads to a hierarchy of equations and boundary conditions that must be solved to each order in ε. To leading order in ε, one recovers the equations encountered for a fluid lying between two straight plates. In this case,

$$u^0 = w^0 = 0, \quad p^0_\eta = \mathrm{Ra}(1-\eta), \quad \theta^0 = 1-\eta. \quad (21)$$

The equations to $O(\varepsilon)$ become

$$u^1_\xi + w^1_\eta = 0, \quad (22)$$

$$-p^1_\xi + aR\mathrm{v}(u^1_{\xi\xi} + u^1_{\eta\eta}) - r^1_\xi - s^1_\eta = -\eta f' p^0_\eta, \quad (23)$$

$$-p^1_\eta + aR\mathrm{v}(w^1_{\xi\xi} + w^1_{\eta\eta}) - s^1_\xi - q^1_\eta + \mathrm{Ra}\theta^1 = -fp^0_\eta, \quad (24)$$

$$w^1\theta^0_\eta - \theta^1_{\xi\xi} - \theta^1_{\eta\eta} = 0, \quad (25)$$

$$s^1 + a(u^1_\eta + w^1_\xi) = 0, \quad (26)$$

$$r^1 + 2au^1_\xi = 0, \quad (27)$$

$$q^1 + 2aw^1_\nu = 0, \quad (28)$$

which must be solved subject to

$$\begin{pmatrix} u^1 \\ w^1 \\ \theta^1 \end{pmatrix}(\xi,\eta=0) = \begin{pmatrix} u^1 \\ w^1 \\ \theta^1 \end{pmatrix}(\xi,\eta=1) = \mathbf{0},$$

$$\mathbf{v}^1(\xi=0,\eta) = \mathbf{v}^1(\xi=2\pi/\alpha,\eta). \quad (29)$$

Note that the first expressions in Eq. (21) have been used. The general solution of the nonhomogeneous system (22)–(28) may be written as

$$\mathbf{v}^1(\xi,\eta) = \sum_{n=1}^{N} \mathbf{v}^{11}_n(\eta)\sin(n\alpha x) + \mathbf{v}^{12}_n(\eta)\cos(n\alpha x). \quad (30)$$

The equations to $O(\varepsilon^2)$ for a non-Newtonian fluid become

$$u^2_\xi + w^2_\eta = nf' u^1_\eta - fw^1_\eta, \quad (31)$$

$$-p^2_\xi - r^2_\xi - s^2_\eta + aR\mathrm{v}(u^2_{\xi\xi} + u^2_{\eta\eta}) = \mathrm{Pr}^{-1}(u^1u^1_\xi + w^1u^1_\eta) - nf' p^1_\eta - \eta f' r^1_\eta - fs^1_\eta - aR\mathrm{v}(-2\eta f' u^1_{\xi\eta} - 2fu^1_{\eta\eta} - nf'' u^1_\eta) + nf' fp^0_\eta, \quad (32)$$

$$-p_\eta^2 - f^2 p_\eta^0 - s_\xi^2 - q_\eta^2 + \mathrm{Ra}\theta^2 + aR\mathrm{v}(w_{\xi\xi}^2 + w_{\eta\eta}^2) = \mathrm{Pr}^{-1}(u^1 w_\xi^1 + w^1 w_\eta^1) - f p_\eta^1 - \eta f' s_\eta^1 - f q_\eta^1 - aR\mathrm{v}(-2\eta f' w_{\xi\eta}^1 - 2f w_{\eta\eta}^1 - n f'' w_\eta^1), \quad (33)$$

$$\theta_{\xi\xi}^2 + \theta_{\eta\eta}^2 - w^2\theta_\eta^0 = -2nf'\theta_{\xi\eta}^1 - 2f\theta_{\eta\eta}^1 - nf''\theta_\eta^1 + nf'^2\theta_\eta^0, u^1\theta_\xi^1 - nf' u^1\theta_\eta^0 + w^1\theta_\eta^1 - f w^1\theta_\eta^0, \quad (34)$$

$$-\mathrm{De}^{-1}(s^2 + a u_\eta^2 + a w_\xi^2) = u^1 s_\xi^1 + w^1 s_\eta^1 - r^1 w_\xi^1 - q^1 u_\eta^1 - a\mathrm{De}^{-1}(f u_\eta^1 + f\eta w_\eta^1), \quad (35)$$

$$-\mathrm{De}^{-1}(r^2 + 2a u_\xi^2) = u^1 r_\xi^1 + w^1 r_\eta^1 - 2r^1 u_\xi^1 - 2s^1 u_\eta^1 - 2a\mathrm{De}^{-1}\eta f' u_\eta^1, \quad (36)$$

$$-\mathrm{De}^{-1}(q^2 + 2a w_\eta^2) = u^1 q_\xi^1 + w^1 q_\eta^1 - 2s^1 w_\xi^1 - 2q^1 w_\eta^1 - 2a\mathrm{De}^{-1} f w_\eta^1, \quad (37)$$

which must be solved subject to

$$\begin{pmatrix} u^2 \\ w^2 \\ \theta^2 \end{pmatrix}(\xi, \eta = 0) = \begin{pmatrix} u^2 \\ w^2 \\ \theta^2 \end{pmatrix}(\xi, \eta = 1) = \mathbf{0},$$

$$\mathbf{v}^2(\xi = 0, \eta) = \mathbf{v}^2(\xi = 2\pi/\alpha, \eta). \quad (38)$$

Note that the first of expressions (21) has been used. The general solution of the nonhomogeneous system (31)–(37) may be written as

$$\mathbf{v}^2(\xi, \eta) = \sum_{m=1}^{M}\sum_{n=1}^{N} \mathbf{v}_{nm}^{21}(\eta)\sin(n+m)\alpha x + \mathbf{v}_{nm}^{22}(\eta)\cos(n+m)\alpha x + \mathbf{v}_{nm}^{23}(\eta)\sin(n-m)\alpha x + \mathbf{v}_{nm}^{24}(\eta)\cos(n-m)\alpha x. \quad (39)$$

The coefficients in expansions (30) and (39) are governed by two sets of ODEs, which are solved using a variable-step finite-difference scheme (subroutine IMSL-DBVPFD in Fortran). The basic discretization is the trapezoidal rule over a nonuniform mesh chosen adaptively so that the local error has approximately the same size everywhere. The linear system of equations is solved using a special form of Gauss elimination that preserves sparseness. At this point, it is necessary to introduce explicitly the modulated wall profile f. Various wall configurations may be easily incorporated, including arbitrary wall shape, as long as the shape is continuous. In this work, however, the upper wall is assumed to be modulated in the form of a cosine wave such that

$$f(\xi) = \cos(\alpha\xi), \quad (40)$$

The corresponding equations in this case for the first and the second order are detailed in Appendixes B and C.

III. RESULTS AND DISCUSSION

In this section, the influence of inertia, elasticity, and modulation parameters is examined on the thermal convection pattern. The numerical assessment of the numerical implementation is also carried out against the finite-volume method for a Newtonian fluid. All results reported below are based on $\mathrm{Pr}=10$. Since the effect of the viscosity ratio is to modify the elastic character of the fluid, only the influence of the Deborah number is examined, with the viscosity ratio fixed to $R_\mathrm{v}=1$.

A. Newtonian flow and numerical assessment

Consider first the modulated thermal convection of a Newtonian fluid. This flow is important, as it constitutes a limit case for the viscoelastic fluid, and will be used for numerical assessment. Recall that for a Newtonian fluid either the first- or second-order solution may be used. In this case, the validity of the first- and second-order solutions will be assessed against the finite-volume method (Fluent), which will be taken as exact. Typically, a grid of 138×40 elements is chosen. Periodic boundary conditions are imposed, with negligible flow rate (10^{-9} kg s^{-1}). The Boussinesq approximation is also imposed. The second-order resolution is chosen, and the convergence criteria are set to 10^{-4} for the momentum and 10^{-6} for the continuity and energy conservation equations. Convergence is typically secured after 700 iterations. It is well established that while the semianalytical first-order perturbation expansion leads to an accuracy in the order of ε^2, this accuracy is improved to order ε^3 for the 2nd order perturbation expansion. Although it may be generally inferred that the qualitative picture remains the same for any order, this may not always be true as will be observed later.

The overall influence of the truncation level is illustrated in Fig. 2, for a Newtonian flow at $\mathrm{Ra}=1200$, $\varepsilon=0.1$, and $\alpha=1.5$. In these figures, the first- and second-order solutions as well as the finite-volume solution are displayed for comparison. The velocity, temperature, and pressure profiles are plotted against z at $x/\lambda=0.43$, and against x/λ at $z=0.3$. These locations are deliberately chosen where the difference among the three methods is greatest. The three methods exhibit the same qualitative picture for all variables except for w. Indeed, the results for the second-order and the finite-volume solutions are very close. The larger discrepancy is found to be for the velocity components u and w between the first- and second-order (or Fluent). This is also confirmed below when the average relative error is examined. The temperature distribution is the same regardless of the solution method. The pressure magnitude is essentially the same for the perturbation methods, but is slightly underestimated.

The accuracy of the numerical implementation is further assessed by monitoring the relative error to each order of the perturbation solution against Fluent. In this case, although the results based on Fluent imply a certain level of inaccuracy, they will be taken to correspond to the exact solution. Figure 3 shows the average relative error in percentage for each variable, namely $\langle e(u)\rangle$, $\langle e(w)\rangle$, $\langle e(\theta)\rangle$, and $\langle e(p)\rangle$ as function of the Rayleigh number. The error is defined, for each variable v, by $e(v)=100|(v^\varepsilon - v^f)/v^f|$, where v^ε and v^f

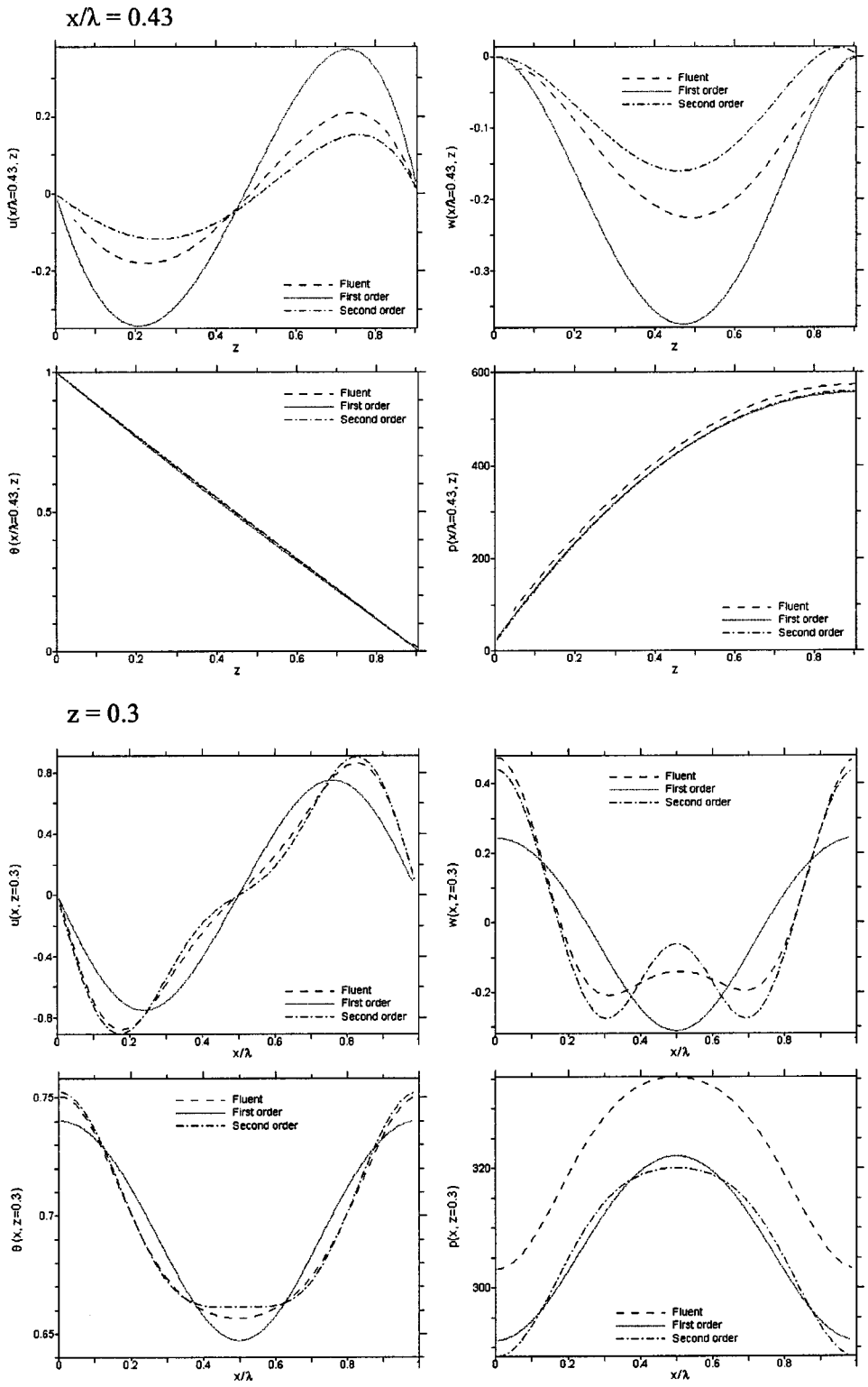

FIG. 2. Streamwise and depthwise velocity, temperature, and pressure distributions at $x/\lambda=0.43$ for Ra=1200, Pr=10, $\varepsilon=0.1$, and $\alpha=1.5$. The figure shows the distributions based on the first-, second-order perturbation, and finite-volume methods.

are the variables based on the perturbation method and the finite-volume method, respectively. In general, there is a significant improvement when the second-order terms are included, reducing the error to less than a few percent. Finally, additional numerical assessment was carried out by monitoring the change in volume flow rate. The flow rate is found to be conserved to within 10^{-6} for both the first- and the second-order perturbation analysis. Given the assessment

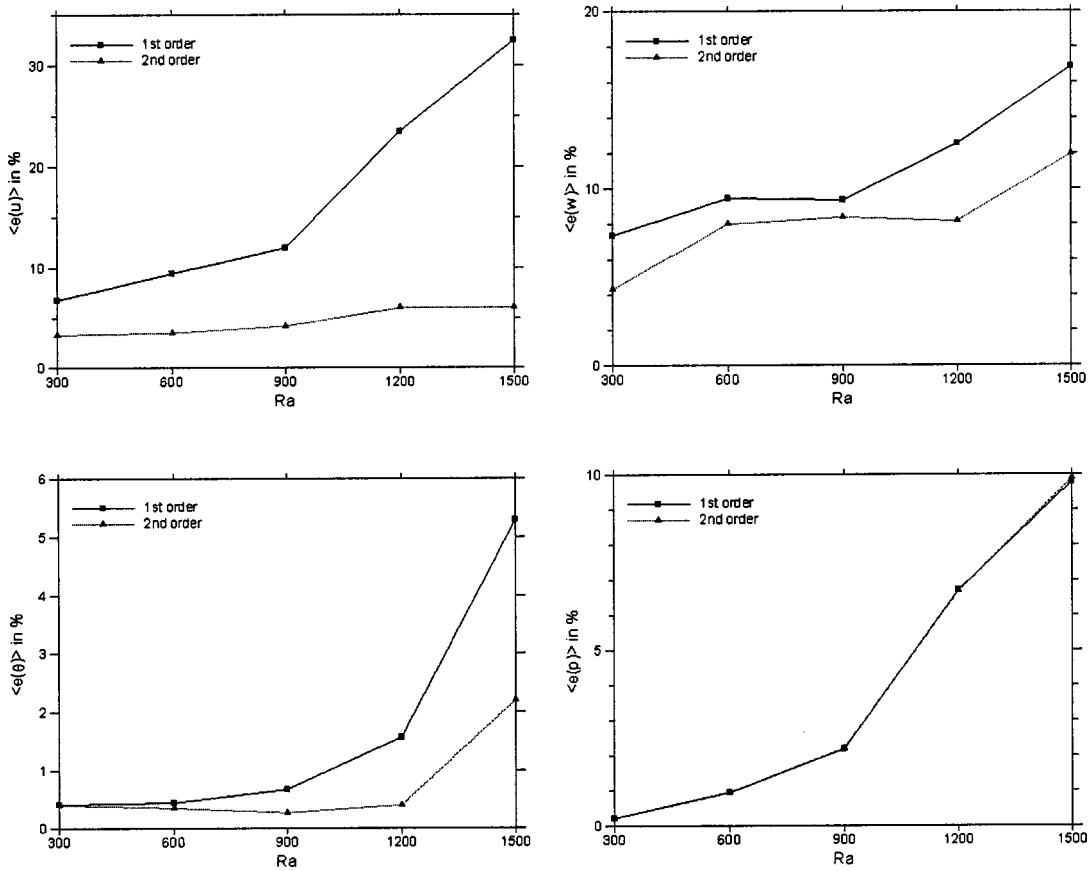

FIG. 3. Average relative error of u, w, θ, and p against Ra for Pr=10, $\varepsilon=0.1$, and $\alpha=1.5$. The figure shows the errors between the perturbation method and the finite-volume method, whose solution is taken as exact.

above, all the results reported below will be based on the second-order perturbation solution.

B. Influence of elasticity

The influence of elasticity is best assessed by varying De and keeping the remaining parameter fixed. The Newtonian flow remains significant in this case, as it constitutes the limit of viscoelastic flow for vanishingly small Deborah number or infinite viscosity ratio. The overall change between Newtonian and non-Newtonian behavior is typically summarized in Fig. 4, which compares the flow and temperature fields for Ra=1200, $\varepsilon=0.1$, and $\alpha=1.5$. Here De=1 for the viscoelastic flow. Note that the same scale is used for each variable for clarity of comparison. A noticeable effect of the elasticity is the distortion of the convective cells, which is particularly evident from the velocity contours. The streamlines indicate that the cells become diamondlike as opposed to circular, and increase in size in the non-Newtonian case. As a result, the downward flow has increased in strength below the trough. Thus elasticity tends to make the cells more symmetrical compared to the Newtonian pattern. Recall from the discussion above that the loss of symmetry is directly related to the strength of the second-order terms. In this case, the higher-order terms induce a loss of symmetry in the velocity rather than the streamlines. Although the temperature remains essentially unaffected by elasticity, the pressure exhibits some modulation in the streamwise direction. The level of distortion depends on both elastic and inertial effects.

The influence of inertia is now examined by varying the Rayleigh number Ra from 300 to 1500, while keeping the other parameters as before. Figure 5 shows the influence of inertia for both Newtonian and non-Newtonian (De=2) fluids. In the Newtonian case, besides the expected increase in flow intensity, the rolls retain their circular shape, and tend to center below the crests, with increasing distance in between, as Ra increases. The relative void below the trough leads eventually to the birth of two new weak vortices of opposite direction. In contrast, in the non-Newtonian case, the rolls tend to distort in shape, approaching one another, as Ra increases. New rolls appear below the crest.

Further quantitative assessment is inferred from Fig. 6, where the velocity, temperature, and pressure distributions are plotted across the channel for the same fluids as in Fig. 5. The horizontal location is fixed at $x/\lambda=0.43$, where non-Newtonian effects can be clearly illustrated. It is clear that an increase in inertia leads generally to an increase in flow intensity. However, in the Newtonian case, it is observed that for Ra$>$1200 the flow intensity diminishes with Ra as a result of the shift in roll position, but eventually significant flow activity is predicted as the new rolls appear. It is interesting to note that the streamwise (depthwise) flow remains essentially antisymmetric (symmetric) with respect to the middle of the roll; the slight loss of symmetry is almost

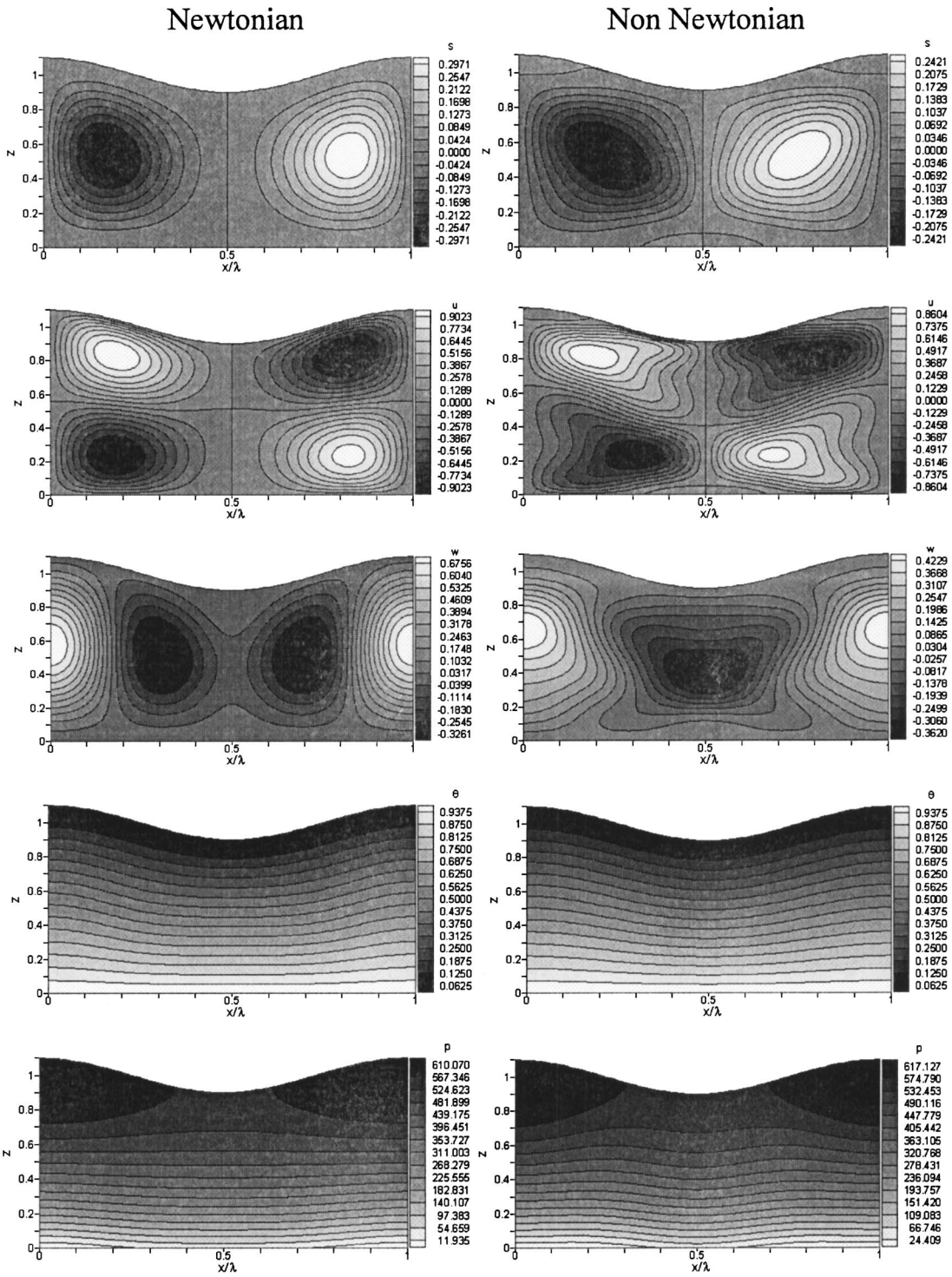

FIG. 4. Comparison of mean flow patterns based on the second-order perturbation method for a Newtonian and a non-Newtonian fluid (De=1 and R_v=1) for Ra=1200, Pr=10, ε=0.1, and α=1.5. The figure displays the streamlines, u, w, θ and p contours.

solely due to wall modulation (see the u and w curves in Fig. 6). In contrast, the symmetry is entirely lost for the non-Newtonian fluid. The flow strengthens monotonically with Ra. Another effect of inertia is the deviation of the temperature from the linear distribution, especially for the viscoelastic fluid. Despite the significant departure in the flow structure between the Newtonian and non-Newtonian fluids as Ra increases, the pressure distribution remains qualitatively the same, with the pressure magnitude being slightly higher for the viscoelastic fluid, particularly near the lower plate. Unlike the flow velocity (see below), the pressure appears to increase only linearly with Ra. The insensitivity to non-Newtonian effect of the pressure can be of important practical significance. In lubrication flow, for instance, the separating force is essentially independent of the level of elasticity of the fluid.

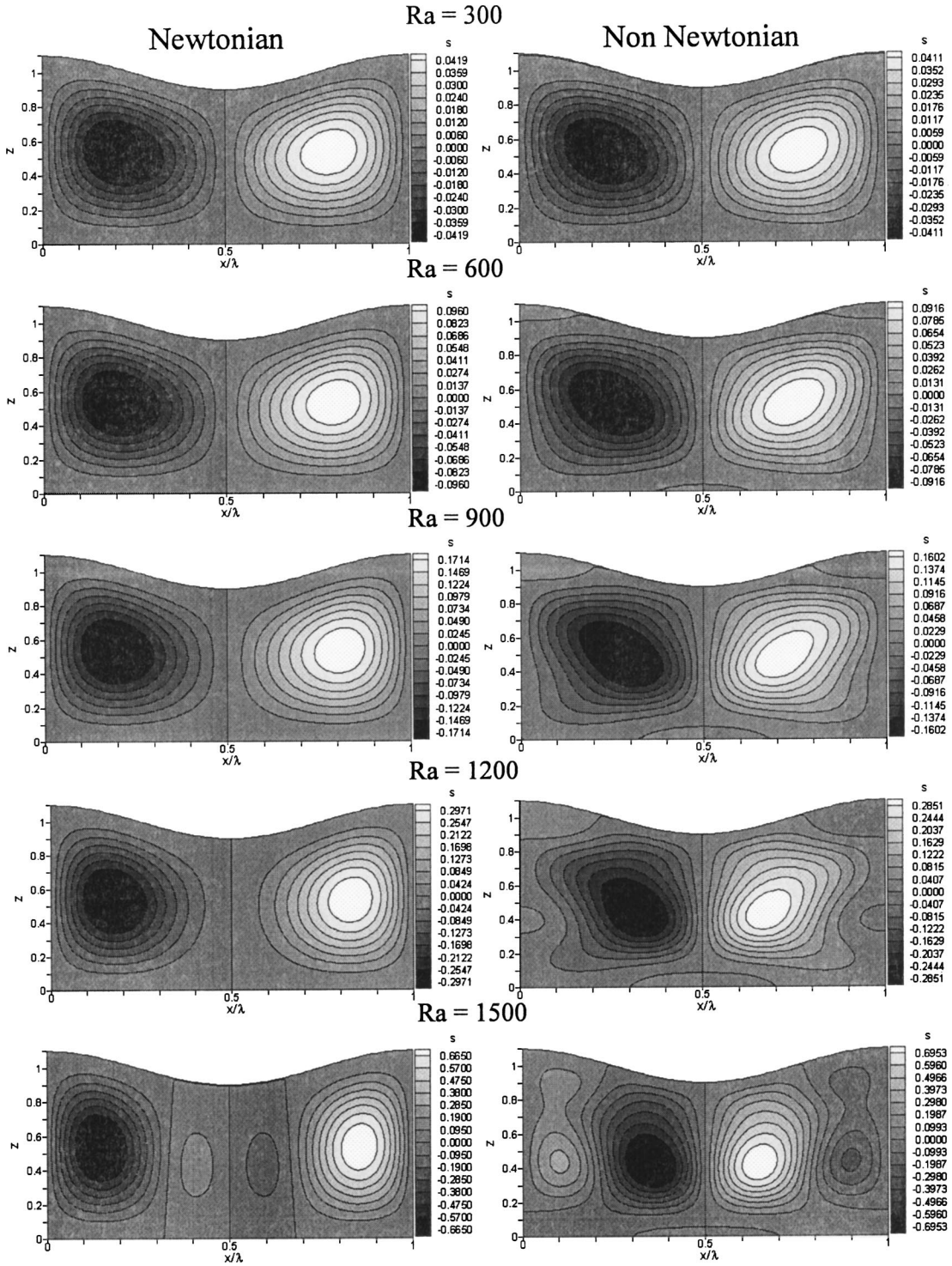

FIG. 5. Influence of inertia on flow streamlines for a Newtonian and a non-Newtonian fluid (De=2 and $R_v=1$) for $\mathrm{Ra}\in[300,1500]$, Pr=10, $\varepsilon=0.1$, and $\alpha=1.5$.

A relevant parameter to examine in the case of convection problems is the Nusselt number Nu which is the ratio of the actual heat transfer to the heat transfer that would occur by conduction alone in the case of steady-state flow between straight plates. In the present problem, the Nusselt number is given as $\mathrm{Nu}(x)=-\partial\theta/\partial y|_{y=0}$. Figure 7 illustrates the variation in Nu against x/λ for several values of Ra. The upper-wall modulation is also shown for reference. It is noted that at Ra=0, Nu is not constantly equal to 1 as one would expect for the flow between parallel plates. In this case, $\mathrm{Nu}(x)_{\mathrm{Ra}=0}=1/1+\varepsilon f(x)$. Generally, for a Newtonian fluid, convection tends to be strongest beneath the crest, in contrast to the case of a viscoelastic fluid where Nu is highest beneath the trough. The appearance of additional peaks and valleys in the Nu distributions corresponds to the emergence of additional rolls (compare Figs. 5 and 7).

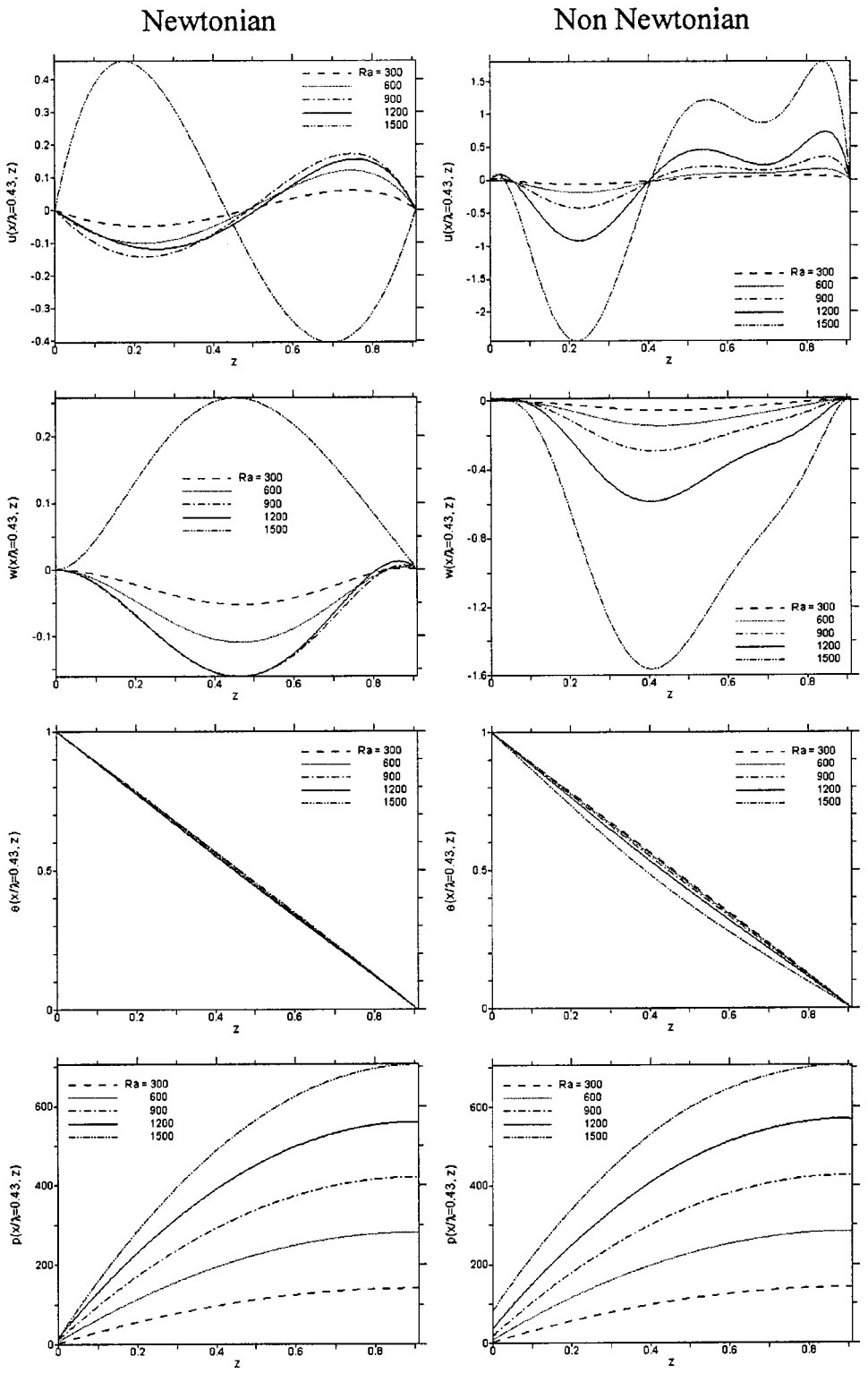

FIG. 6. Influence of inertia on u, w, θ, and p distributions for a Newtonian and a non-Newtonian fluid (De=2 and R_v=1) at x/λ =0.43 for Ra $\in$ [300,1500], Pr=10, ε=0.1, and α=1.5.

The influence of elasticity on the flow is examined next by varying the Deborah number De, for a flow at Ra = 1200, keeping the remaining parameters as before. Figure 8 shows the change in flow structure as De increases. The major departure from Newtonian behavior is in the form of roll distortion and the birth of the additional rolls below the crests. Recall that viscoelastic effects are of second order and higher in ε. As De increases, it is then expected that the flow becomes increasingly modulated, as expressions (39) suggest. The additional modulation corresponds to a wavelength

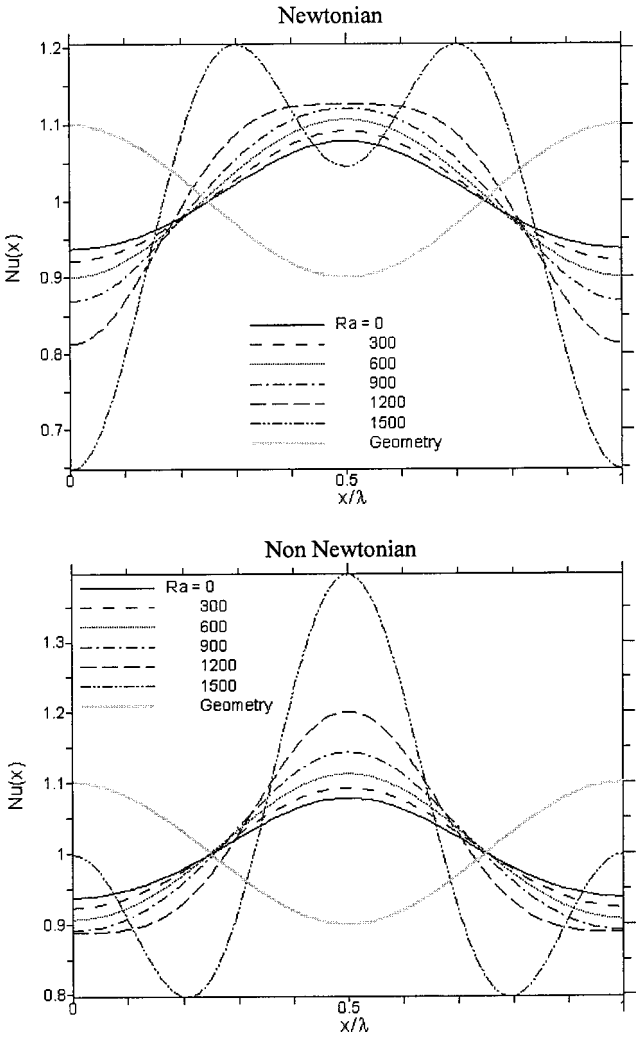

FIG. 7. Influence of inertia on the Nusselt number distribution along the channel, Nu(x), for a Newtonian and a non-Newtonian fluid (De=2 and R_v=1) for Ra$\in[0,1500]$, Pr=10, ε=0.1, and α =1.5. The gray solid line represents the upper wall geometry.

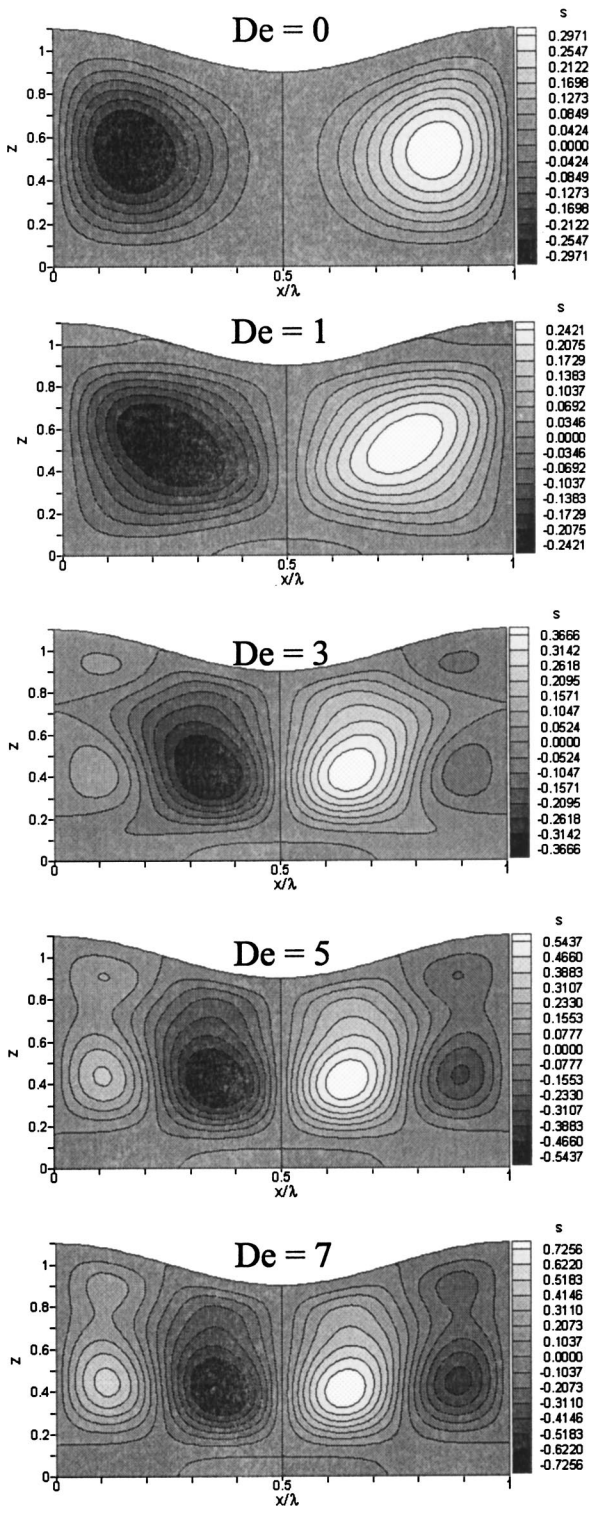

FIG. 8. Influence of elasticity on flow streamlines for De $\in[0,7]$, R_v=1, Ra=1200, Pr=10, ε=0.1, and α=1.5.

equal to half that of the wall, which explains that four rolls can be accommodated at De=7 in the case of a viscoelastic fluid.

The elasticity-enhanced distortion and additional modulation are clearly confirmed in Fig. 9. The modulation, however, is only visible in the velocity distributions. The effect of elasticity tends to be limited concerning the temperature, which shows small deviation from linear behavior. Similarly, the pressure increases only slightly and linearly with De, confirming the earlier observation that fluid elasticity is essentially uninfluential on the pressure.

The overall interplay between inertia and elasticity is interesting to examine. For this purpose, the influence of both Ra and De is assessed on the maximum of the velocity magnitude $|u,w|_{\max}=\max[\sqrt{(u^2+w^2)}]$, which is taken to reflect the flow intensity. Figure 10 shows projections over the ranges De$\in[0,5]$ and Ra$\in[30,1500]$. While the increase in flow intensity with Ra is monotonic, it is piecewise linear with respect to De. A remarkable feature in Fig. 10 is the absence of elasticity influence at low Rayleigh number. As Ra increases, the flow intensity increases slightly with De. At large Ra, the flow intensity exhibits a minimum.

The overall influence of both inertia and elasticity on the thermal convection is examined by assessing the dependence of the mean Nusselt number,

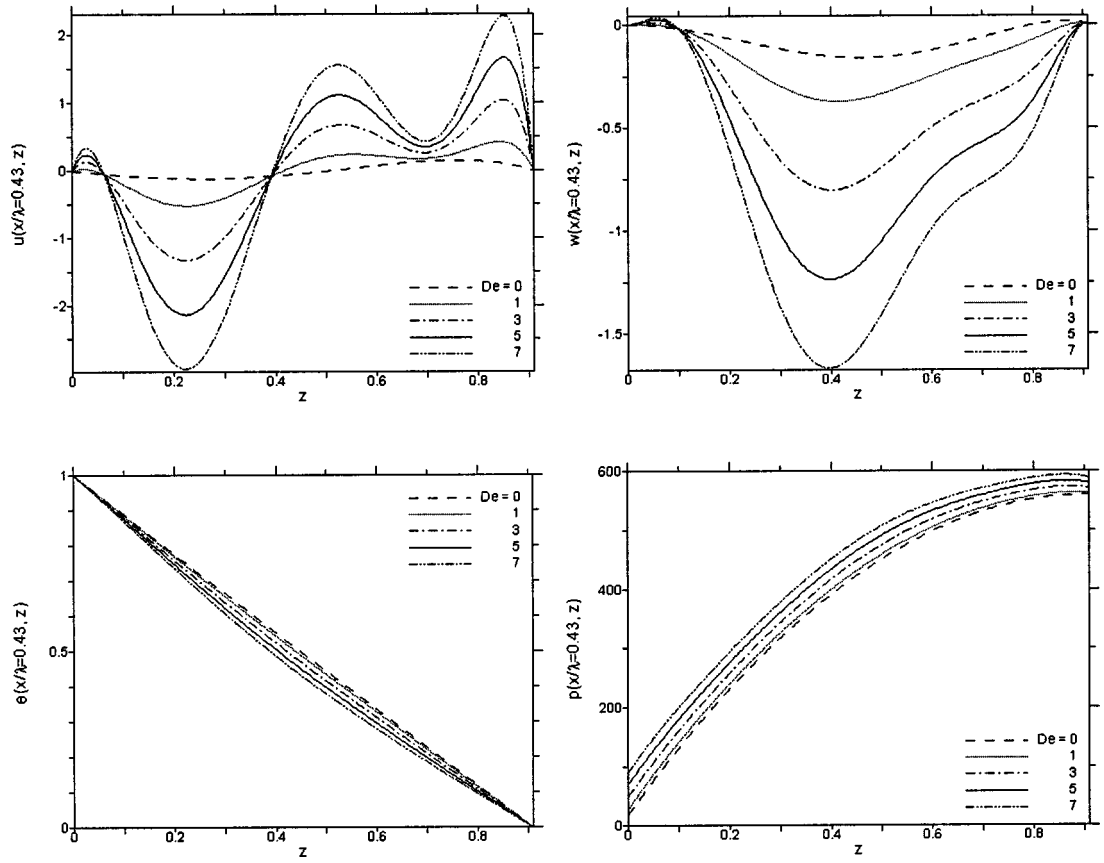

FIG. 9. Influence of elasticity on u, w, θ, and p distributions for $\mathrm{De}\in[0,7]$, $R_v=1$, $\mathrm{Ra}=1200$, $\mathrm{Pr}=10$, $\varepsilon=0.1$, and $\alpha=1.5$.

$$\langle \mathrm{Nu}\rangle = \frac{\alpha}{2\pi}\int_0^{2\pi/\alpha} \mathrm{Nu}(x)dx,$$

on Ra and De, as illustrated in Fig. 11. It is found that $\langle \mathrm{Nu}\rangle$ increases linearly with De, at any Ra. For small $\mathrm{Ra}(\mathrm{Ra}<1200)$, the mean Nusselt number is essentially independent of De. This is an interesting prediction since it states that, while Nu changes *locally* drastically between the Newtonian and non-Newtonian cases (see Fig. 7), suggesting a strong difference in the local heat convection, Fig. 11 clearly indicates that the *overall* heat convection is unaffected by elasticity for most of the practical range of Rayleigh numbers. For the highest Ra level considered ($\mathrm{Ra}=1500$), the change in $\langle \mathrm{Nu}\rangle$ is 25% between a Newtonian fluid ($\mathrm{De}=0$) and a strongly elastic fluid ($\mathrm{De}=5$). In contrast, the influence of Ra on the overall convection is strong, as $\langle \mathrm{Nu}\rangle$ has nearly tripled when Ra is increased from 30 to 1500.

C. Influence of modulation geometry

The effect of the modulation geometry is best assessed by varying the modulation wave number α and amplitude ε. The influence of these two parameters on the flow pattern is expected to be significant since they dictate the level of coupling between the leading and higher-order perturbation terms. Relatively strong values of α and ε unavoidably lead to nonlinear enhancement.

The overall influence of α is reflected in Fig. 12, where the streamlines are displayed for both a Newtonian and a non-Newtonian fluid at for $\varepsilon=0.1$, $\mathrm{Ra}=1200$, and $\mathrm{De}=2$. In the Newtonian case, an increase in α causes the rolls to occupy an increasingly higher portion of the flow. The rolls tend to embrace the shape of the two walls while simultaneously invading the area beneath the trough (see the case $\alpha=5$). In contrast, the convection of a non-Newtonian fluid exhibits a significant distortion of the rolls, leading to the birth of secondary vortices beneath the crest near the upper wall, beneath the trough near the lower wall, and on the sides (see the case $\alpha=3$). This behavior is enhanced by elasticity (not shown). As α increases further, the secondary vortices disappear by merging together, resulting in a pattern similar to the one for low α (compare the case $\alpha=5$ and $\alpha=1$).

The profiles in Fig. 13 confirm the consistency in the Newtonian roll structure; all velocity, temperature, and pressure profiles remain unaltered in shape as α changes. In the non-Newtonian case, it is interesting to observe that the velocity profiles are modulated for any α value; however, the modulation amplitude is vanishingly small for small and large wave number. Although the temperature displays the same response as for a Newtonian fluid, the pressure exhibits weak modulation, which is particularly visible for $\alpha=3$.

The overall interplay between the modulation number and elasticity is summarized in Figs. 14 and 15. The flow intensity exhibits a maximum at a wave number slightly smaller than 3, which is sensibly the same for any level of elasticity. Thus, this is the optimal wave number that is required to

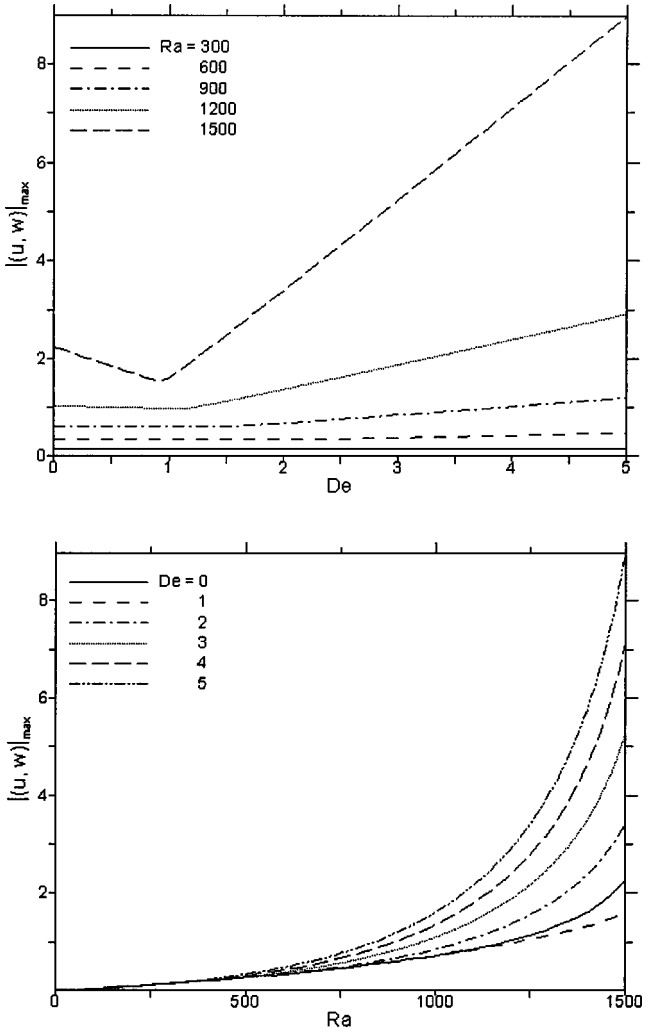

FIG. 10. Influence of elasticity and inertia on the maximum velocity magnitude, $|(u,w)|_{\max}$, for $\mathrm{De}\in[0,5]$, $\mathrm{Ra}\in[30,1500]$, $R_v=1$, $\mathrm{Pr}=10$, $\varepsilon=0.1$, and $\alpha=1.5$.

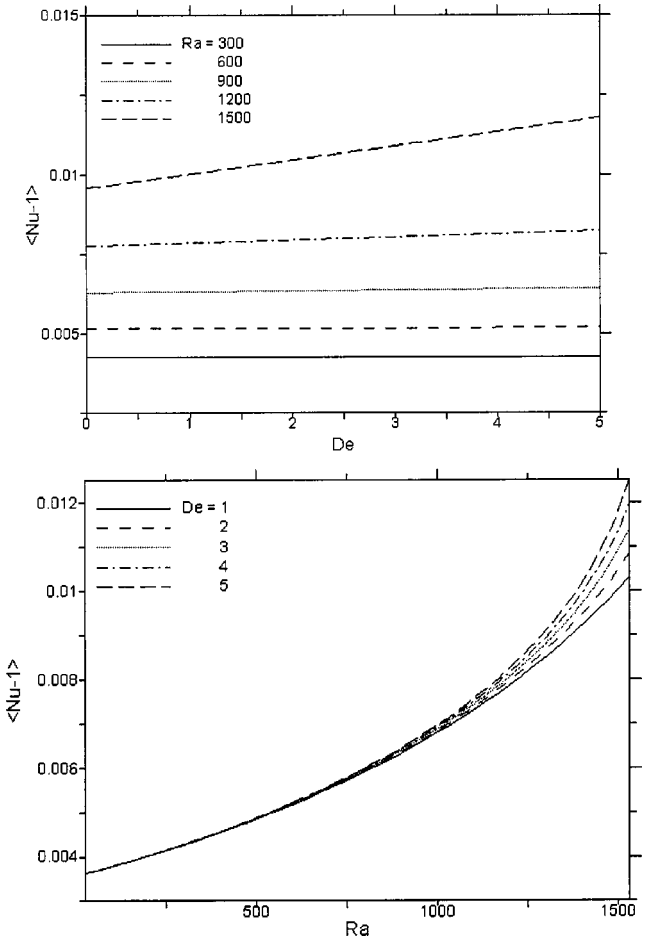

FIG. 11. Influence of elasticity and inertia on the average Nusselt number, $\langle \mathrm{Nu}-1\rangle$, for $\mathrm{De}\in[0,5]$, $\mathrm{Ra}\in[30,1500]$, $R_v=1$, $\mathrm{Pr}=10$, $\varepsilon=0.1$, and $\alpha=1.5$.

observe the convective pattern in practice, regardless of the fluid used. Elasticity simply enhances monotonically the flow intensity (see Fig. 14). This enhancement depends strongly on α, and seems to be greatest for α close to 3 (see bottom of Fig. 14). The average Nusselt number in Fig. 15 shows that the overall convection remains unaffected by fluid elasticity for any wave number. This is also confirmed from the lower right-hand figure, which shows that the dependence of heat convection on α is dictated by a universal curve. This universal character is in sharp contrast when the dependence of thermal convection on Ra is examined (not shown). At low Ra, for instance, $\langle \mathrm{Nu}\rangle$ does not even exhibit a maximum with α.

The overall influence of the wall modulation amplitude ε is illustrated in Fig. 16 for $\mathrm{Ra}=1200$ and $\alpha=1.5$. From this figure, it is seen that ε has a marked effect on the flow pattern, which is similar to the effect of inertia on both the Newtonian and viscoelastic fluids (compare with Fig. 5). Thus, the increase in modulation amplitude causes a similar response as the increase in inertia: roll distortion and birth of new rolls. There is, however, a significant difference in the pressure. Figure 16 indicates that an increase in Ra leads to linear increase in p. Additional calculations show that p is sensibly independent of ε. The pressure is then predicted to increase with temperature (difference), but remains unaffected by modulation amplitude. Figure 17 displays the dependence of the flow intensity on De and ε. The flow intensity grows with ε. The growth rate is found to be independent of De for weakly elastic fluids, but increases sharply for strongly elastic fluids (compare Figs. 10 and 17). Finally, the similarity between the effects of inertia and modulation amplitude is evident upon inspecting the average Nusselt number in Fig. 18 (compare with Fig. 11).

IV. CONCLUSION

The thermal convection of a viscoelastic fluid inside a weakly modulated channel is investigated throughout the present work. The governing equations are mapped onto a rectangular domain. The ratio ε of the modulation amplitude to the mean channel width emerges as the perturbation parameter, allowing a regular perturbation expansion to be used. A comparative assessment for a Newtonian fluid is car-

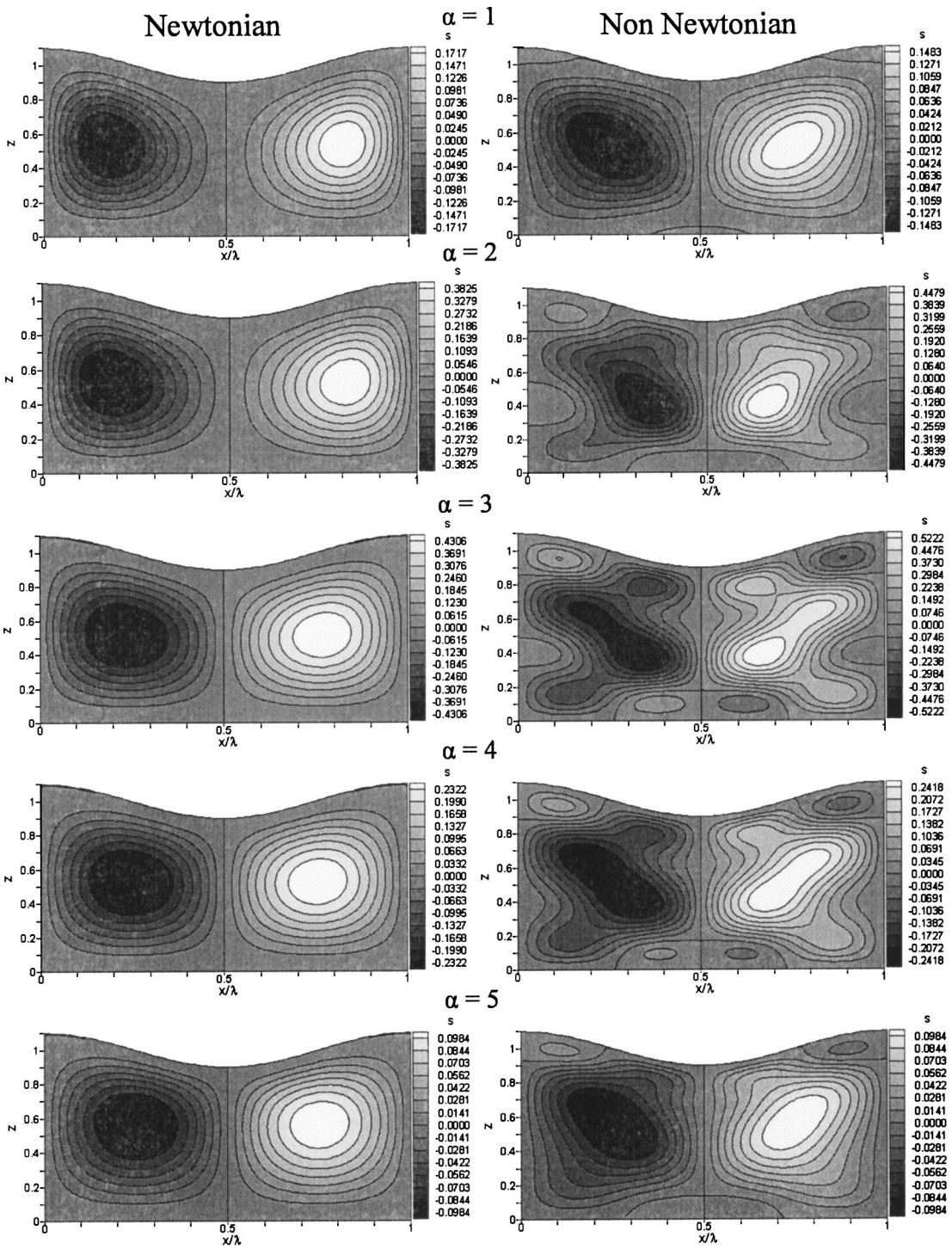

FIG. 12. Influence of wall modulation wave number α on flow streamlines for a Newtonian and a non-Newtonian fluid (De=2 and R_v=1) for $\alpha \in [1,5]$, Ra=1200, Pr=10, and ε=0.1.

ried out against results based on a two-dimensional finite-volume code (Fluent). In addition to being more accurate, the second-order perturbation method reveals new physical phenomena that could not be determined by the first-order perturbation analysis.

As inertia increases, elasticity tends to restore the symmetry in the streamlines but enhances the lack of symmetry in velocity. For a non-Newtonian fluid, rolls are distorted as Ra increases and tend to move near the trough. In contrast, the Newtonian rolls retain their circular shape and tend to center below the crests (Fig. 5). The flow intensity and the global heat transfer, represented, respectively, by the maximum of the velocity magnitude and the average of the Nusselt number, exhibit a maximum at a wave number close to 3, which is sensibly the same for any level of elasticity (Fig. 14 and 16). It is also predicted that the modulation amplitude and inertia have similar effects on both Newtonian and viscoelastic fluids. The pressure is found to be essentially independent

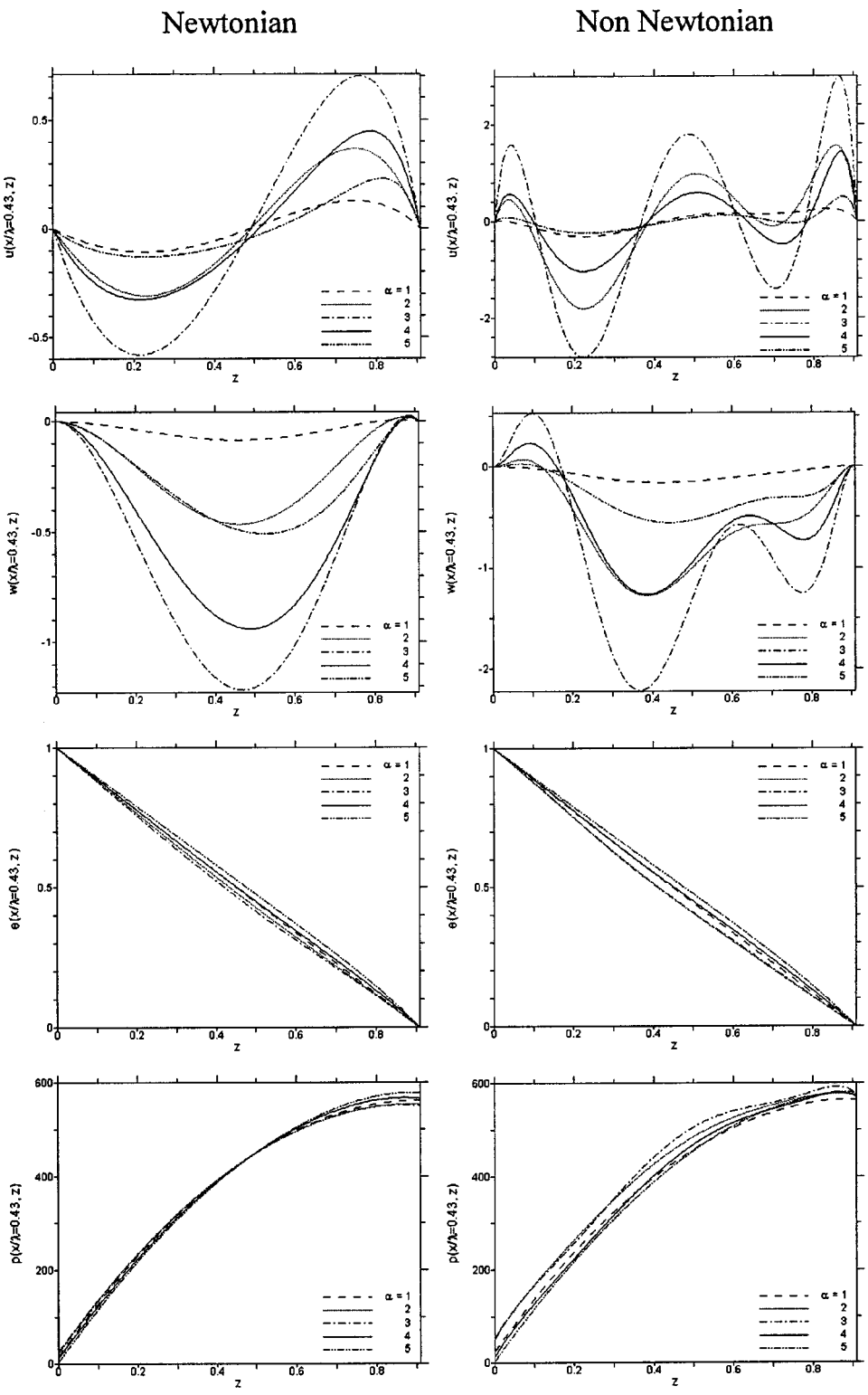

FIG. 13. Influence of wall modulation wave number on u, w, θ, and p distributions for a Newtonian and a non-Newtonian fluid (De $=2$ and $Rv=1$) for $\alpha \in [1,5]$, Ra$=1200$, Pr$=10$, and $\varepsilon=0.1$.

of the fluid elasticity and of the wall modulation wave number and amplitude, which can be of practical relevance to lubrication flow, for instance. Regarding the heat transfer, which is more related to the design of heat exchangers, it can be inferred from the present results that despite strong local changes, the overall heat convection is also unaffected by elasticity for most of the practical range of Rayleigh numbers and for low wall modulation amplitudes.

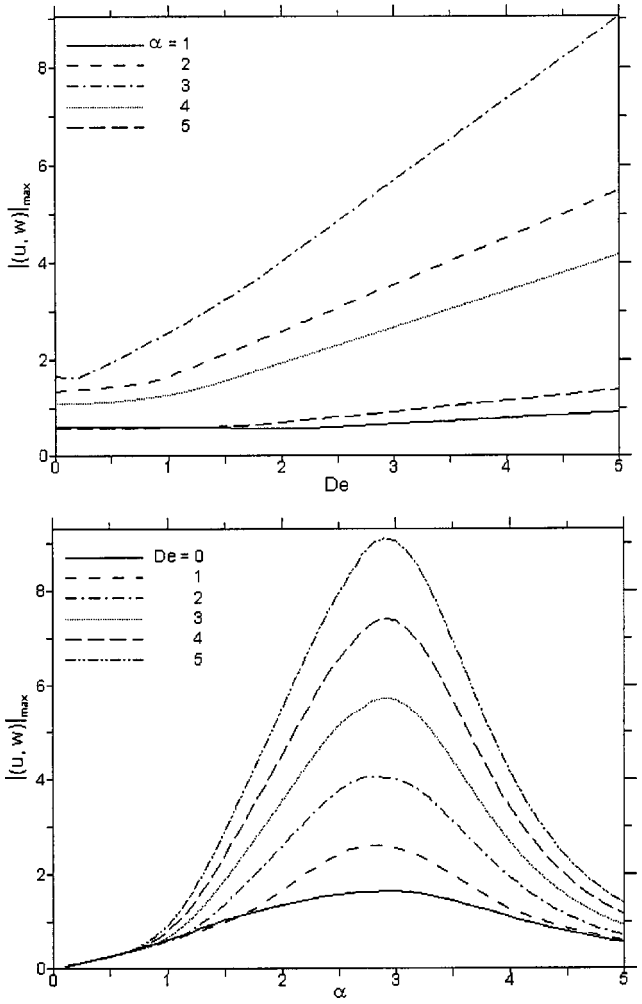

FIG. 14. Influence of elasticity and wall modulation wave number on the maximum velocity magnitude, $|(u,w)|_{\max}$, for De $\in[0,5]$, $\alpha\in[0.1,5]$, $R_v=1$, Ra=1200, Pr=10, and $\varepsilon=0.1$.

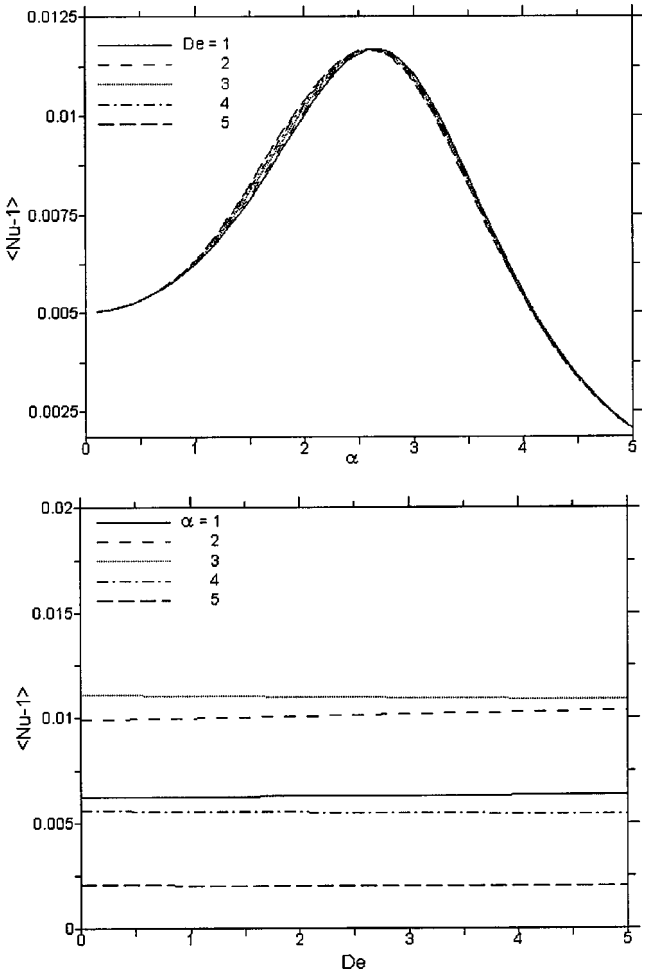

FIG. 15. Influence of elasticity and wall modulation wave number on the average Nusselt number, $\langle \mathrm{Nu}-1\rangle$, for De $\in[0,5]$, $\alpha\in[0.1,5]$, $R_v=1$, Pr=10, and $\varepsilon=0.1$.

In closing, the present results show that elasticity has a marked effect on fluid patterns, especially regarding the roll structure and symmetry. The elasticity appears to be influential when Ra and ε are relatively large, particularly for a wave number $\alpha\approx 3$. One of the major motivations behind the present study is to stimulate further experimental interest in the important area of modulated viscoelastic flow.

ACKNOWLEDGEMENT

The support of the Natural Science and Engineering Research Council of Canada, and that of the Ecole Centrale de Nantes are gratefully acknowledged.

APPENDIX A: TRANSFORMED EQUATIONS AND BOUNDARY CONDITIONS

The transformed equations, based on the mapping (19), read,

$$u_\xi + w_\eta + \varepsilon(-\eta f' u_\eta - f w_\eta) + \varepsilon^2(\eta f f' u_\eta + f^2 w_\eta) = 0, \tag{A1}$$

$$\begin{aligned}\mathrm{Pr}^{-1}&[u u_\xi + w u_\eta + \varepsilon(-\eta f' u u_\eta - f w u_\eta)\\ &+ \varepsilon^2(\eta f f' u u_\eta + f^2 w u_\eta)]\\ =&-P_\xi + a\mathrm{Rv}(u_{\xi\xi}+u_{\eta\eta}) - r_\xi - s_\eta + \varepsilon[\eta f' P_\eta\\ &+ a\mathrm{Rv}(-2f'\,u_{\xi\eta} - 2f u_{\eta\eta} - \eta f'' u_\eta) + \eta f' r_\eta + f s_\eta]\\ &+ \varepsilon^2(-\eta f f'\,P_\eta + a\mathrm{Rv}\,\eta f'^2 u_\eta - f^2 s_\eta - \eta f f' r_\eta),\end{aligned} \tag{A2}$$

$$\begin{aligned}\mathrm{Pr}^{-1}&[u w_\xi + w w_\eta + \varepsilon(-\eta f' u w_\eta - f w w_\eta)\\ &+ \varepsilon^2(\eta f f' u w_\eta + f^2 w w_\eta)]\\ =&-P_\eta + a\mathrm{Rv}(w_{\xi\xi}+w_{\eta\eta}) - s_\xi - q_\eta + \mathrm{Ra}\theta\\ &+ \varepsilon[f P_\eta + a\mathrm{Rv}(2\eta f'\,w_{\xi\eta} + 2f w_{\eta\eta} + \eta f'' w_\eta)\\ &+ \eta f' s_\eta + f q_\eta]\\ &+ \varepsilon^2[-f^2 P_\eta + a\mathrm{Rv}\,\eta f'^2 w_\eta - f f'\,\eta s_\eta - f^2 q_\eta],\end{aligned} \tag{A3}$$

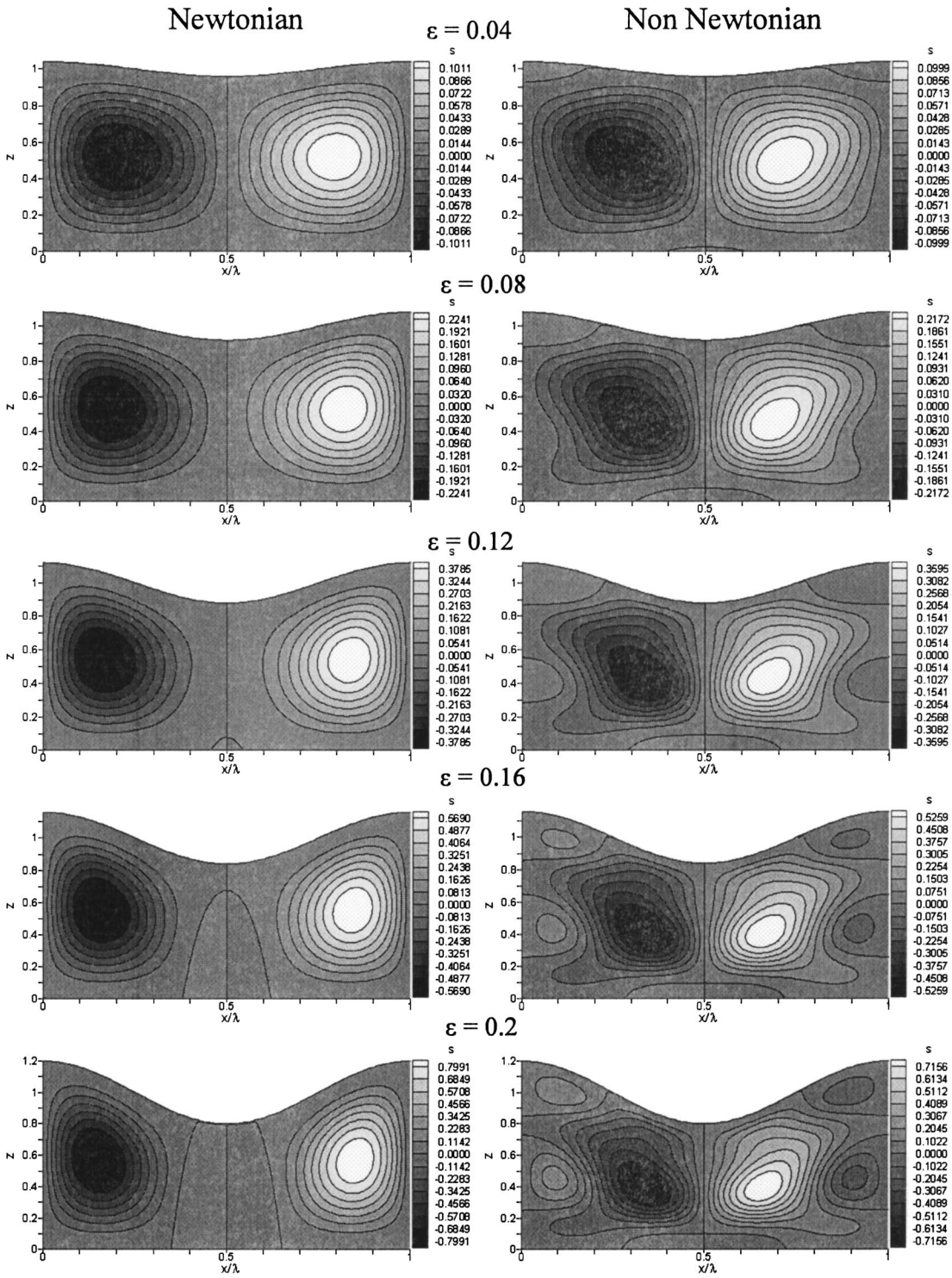

FIG. 16. Influence of wall modulation amplitude ε on flow streamlines for a Newtonian and a non-Newtonian fluid (De=2 and R_v=1) for $\varepsilon \in [0.04, 0.2]$, Ra=1200, Pr=10, and α=1.5.

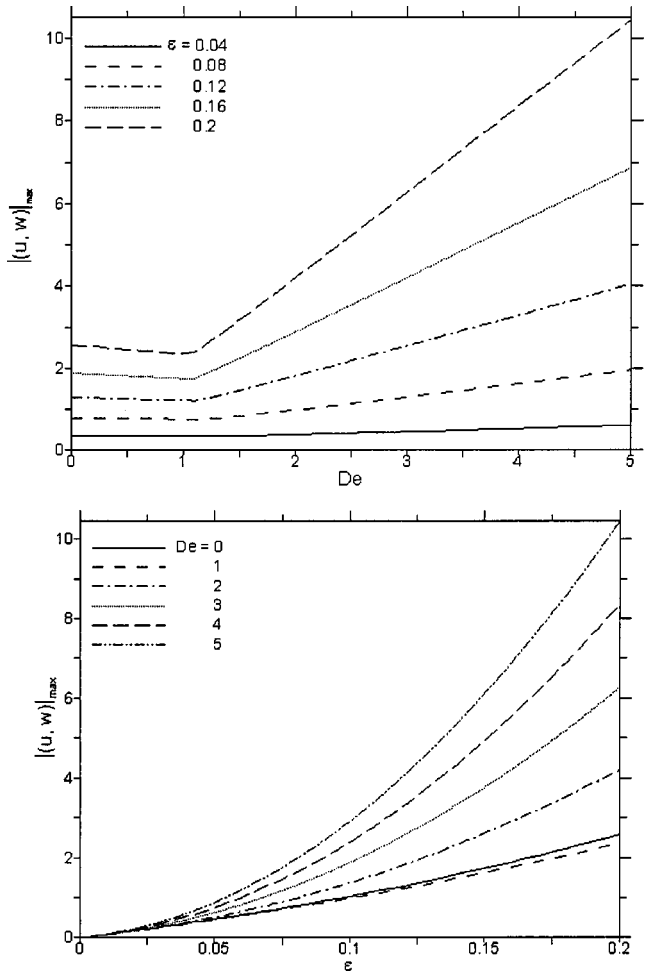

FIG. 17. Influence of elasticity and wall modulation amplitude on the maximum velocity magnitude, $|(u,w)|_{\max}$, for $\mathrm{De}\in[0,5]$, $\varepsilon\in[0.004,0.2]$, $R_v=1$, $\mathrm{Ra}=1200$, $\mathrm{Pr}=10$, and $\alpha=1.5$.

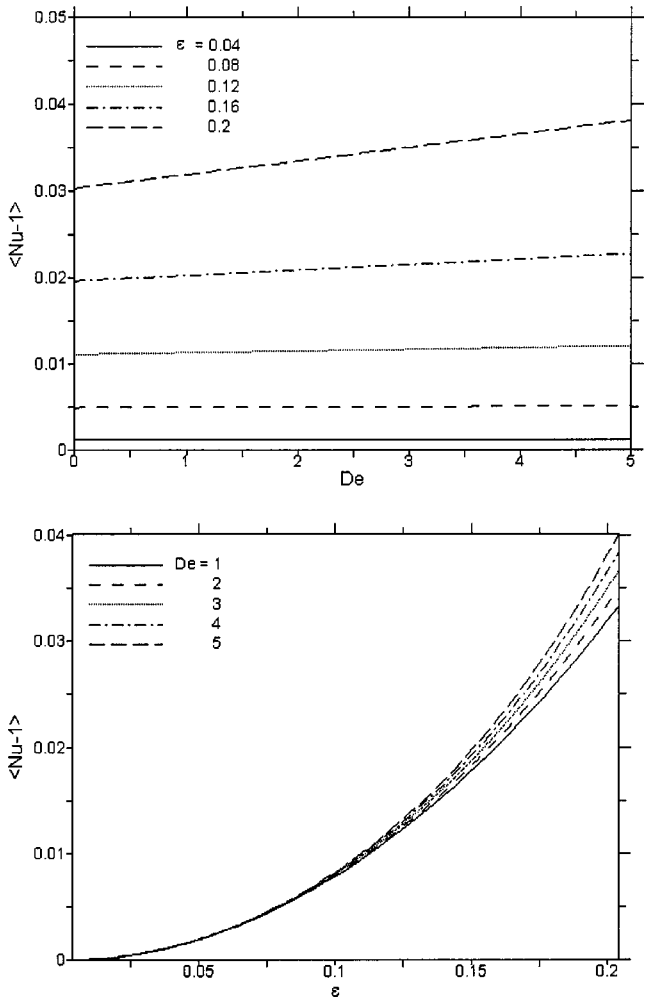

FIG. 18. Influence of elasticity and wall modulation amplitude on the average Nusselt number, $\langle \mathrm{Nu}-1\rangle$, for $\mathrm{De}\in[0,5]$, $\varepsilon\in[0.004,0.2]$, $R_v=1$, $\mathrm{Pr}=10$, and $\alpha=1.5$.

$$u\theta_\xi + w\theta_\eta + \varepsilon(-\eta f' u\theta_\eta - fw\theta_\eta) + \varepsilon^2(\eta ff' u\theta_\eta + f^2 w\theta_\eta) = \theta_{\xi\xi} + \theta_{\eta\eta} + \varepsilon(-2\eta f'\theta_{\xi\eta} - 2f\theta_{\eta\eta} - \eta f''\theta_\eta) + \varepsilon^2[\theta_{\eta\eta}(3f^2 + \eta^2 f'^2) + \eta f'^2\theta_\eta], \quad \text{(A4)}$$

$$us_\xi + ws_\eta - rw_\xi - qu_\eta + \varepsilon(-\eta f' us_\eta - fws_\eta + fqu_\eta - \eta f' rw_\eta) + \varepsilon^2(ff'\eta us_\eta + f^2 ws_\eta - f^2 qu_\eta + ff'\eta rw_\eta) = -\mathrm{De}^{-1}[s + a(u_\eta + w_\xi) + \varepsilon(-afu_\eta - af'\eta w_\eta) + \varepsilon^2(af^2 u_\eta + aff'\eta w_\eta)], \quad \text{(A5)}$$

$$ur_\xi + wr_\eta - 2ru_\xi + 2su_\eta + \varepsilon(-\eta f' ur_\eta - fwr_\eta + 2fsu_\eta + 2\eta f' ru_\eta) + \varepsilon^2(ff'\eta ur_\eta + f^2 wr_\eta - 2f^2 su_\eta - 2ff'\eta ru_\eta) = -\mathrm{De}^{-1}[r + 2au_\xi - \varepsilon 2af'\eta u_\eta + \varepsilon^2 2aff'\eta u_\eta], \quad \text{(A6)}$$

$$uq_\xi + wq_\eta - 2qw_\eta - 2sw_\xi + \varepsilon(-\eta f' uq_\eta - fwq_\eta + 2fqw_\eta + 2\eta f' sw_\eta) + \varepsilon^2(ff'\eta uq_\eta + f^2 wq_\eta - 2f^2 qw_\eta - 2ff'\eta sw_\eta) = -\mathrm{De}^{-1}(q + 2aw_\eta - \varepsilon 2afw_\eta + \varepsilon^2 2af^2 w_\eta), \quad \text{(A7)}$$

where a prime denotes total differentiation. The boundary and periodicity conditions are written as

$$u(\xi,\eta=0) = u(\xi,\eta=1) = 0, \quad w(\xi,\eta=0) = w(\xi,\eta=1) = 0,$$

$$\theta(\xi,\eta=0) = 1, \quad \theta(\xi,\eta=1) = 0,$$

$$u(\xi=0,\eta) = u(\xi=2\pi/\alpha,\eta), \quad w(\xi=0,\eta) = w(\xi=2\pi/\alpha,\eta),$$

$$\theta(\xi=0,\eta) = \theta(\xi=2\pi/\alpha,\eta), \quad p(\xi=0,\eta) = p(\xi=2\pi/\alpha,\eta),$$

$$q(\xi=0,\eta) = q,(\xi=2\pi/\alpha,\eta), \quad r(\xi=0,\eta) = r(\xi=2\pi/\alpha,\eta),$$

$$s(\xi=0,\eta) = s(\xi=2\pi/\alpha,\eta). \quad \text{(A8)}$$

APPENDIX B: EQUATIONS FOR THE FIRST-ORDER COEFFICIENTS

Given the sinusoidal shape of the wall, expression (40), expansion (30) reduces to

$$\mathbf{v}^1 = \mathbf{v}^{11}(\eta)\sin(\alpha x) + \mathbf{v}^{12}(\eta)\cos(\alpha x), \tag{B1}$$

where $\mathbf{v}^1$ is the vector containing the variables of the first-order perturbation method, $\mathbf{v}^{11}$ and $\mathbf{v}^{12}$ are vectors of unknown coefficients. It should be noted that the streamwise velocity component is antisymmetric with respect to $x=\lambda/2$ while other variables are symmetric. Therefore, some terms vanish in the general solution of Eqs. (22)–(28) leading to

$$u^1(x,\eta) = \overline{u^1}(\eta)\sin(\alpha x), w^1(x,\eta) = \overline{w^1}(\eta)\cos(\alpha x),$$

$$p^1(x,\eta) = \overline{p^1}(\eta)\cos(\alpha x), \theta^1(x,\eta) = \overline{\theta^1}(\eta)\cos(\alpha x), \tag{B2}$$

where $\overline{u^1}$, $\overline{w^1}$, $\overline{p^1}$, and $\overline{\theta^1}$ are unknown coefficients. Substituting the above expressions into Eqs. (22)–(28), the governing equations for the first-order coefficients become

$$\overline{u^1}_{\eta\eta} + \alpha\overline{p^1} - \alpha^2\overline{u^1} = \eta(1-\eta)\alpha\mathrm{Ra}, \tag{B3}$$

$$\overline{w^1}_{\eta} + \alpha\overline{u^1} = 0, \tag{B4}$$

$$\overline{p^1}_{\eta} + \alpha^2\overline{w^1} - \mathrm{Ra}\,\overline{\theta^1} + \alpha\overline{u^1}_{\eta} = \mathrm{Ra}(1-\eta), \tag{B5}$$

$$\overline{\theta^1}_{\eta\eta} + \overline{w^1} - \alpha^2\overline{\theta^1} = \alpha^2\eta. \tag{B6}$$

Note that q^1, r^1, and s^1 in Eqs. (23) and (24) have been expressed in terms of u^1 and w^1 [see Eqs. (26)–(28)]. The system above is a set of nonhomogeneous ordinary differential equations, which together with the corresponding homogeneous boundary conditions

$$\begin{pmatrix} \overline{u^1} \\ \overline{w^1} \\ \overline{\theta^1} \end{pmatrix}(\eta=0) = \begin{pmatrix} \overline{u^1} \\ \overline{w^1} \\ \overline{\theta^1} \end{pmatrix}(\eta=1) = 0, \tag{B7}$$

constitutes a boundary-value problem of the two-point type.

APPENDIX C: EQUATIONS FOR THE SECOND-ORDER COEFFICIENTS

For sinusoidal wall modulation, expansion (39) reduces to

$$\mathbf{v}^2 = \mathbf{v}^{21}(\eta)\sin(2\alpha x) + \mathbf{v}^{22}(\eta)\cos(2\alpha x), \tag{C1}$$

where $\mathbf{v}^2$ is the vector containing the variables of the second-order perturbation method, $\mathbf{v}^{21}$ and $\mathbf{v}^{22}$ are vectors of unknown coefficients. Given the symmetry of w, θ, p, and the antisymmetry of u with respect to the line $x=\lambda/2$, the general solution of Eqs. (31)–(37) can be written as

$$u^2(x,\eta) = \overline{u^2}(\eta)\sin(2\alpha x), \quad w^2(x,\eta) = \overline{w^2}(\eta)\cos(2\alpha x),$$

$$p^2(x,\eta) = \overline{p^2}(\eta)\cos(2\alpha x), \quad \theta^2(x,\eta) = \overline{\theta^2}(\eta)\cos(2\alpha x), \tag{C2}$$

where, $\overline{u^2}$, $\overline{w^2}$, $\overline{p^2}$, and $\overline{\theta^2}$ are unknown coefficients. Substituting expressions (C2) into Eqs. (31)–(37), the governing equations for the second-order coefficients in the non-Newtonian case become

$$\overline{w^2} + 2\alpha\overline{u^2} = \frac{\alpha}{2}(\eta\overline{u^1}_{\eta} - \overline{u^1}), \tag{C3}$$

$$\begin{aligned}\overline{u^2}_{\eta\eta} + 2\alpha\overline{p^2} - 4\alpha^2\overline{u^2} = {} & \frac{\mathrm{Pr}^1}{2}(\alpha\overline{u^1}^2 + \overline{w^1}\overline{u^1}_{\eta}) + \frac{\alpha\eta\overline{p^1}_{\eta}}{2} \\ & - \frac{\alpha\eta(1-\eta)\mathrm{Ra}}{2} - \frac{3}{2}\alpha^2\eta\overline{u^1}_{\eta} + \overline{u^1}_{\eta\eta} \\ & - \frac{a\overline{w^1}\overline{u^1}_{\eta\eta\eta}}{2} \\ & - \mathrm{De}\; a\alpha\left[- \frac{11}{2}\overline{u^1}_{\eta}^2 - \alpha\overline{w^1}\overline{u^1}_{\eta} + 5\alpha^2\overline{u^1}^2 \right],\end{aligned} \tag{C4}$$

$$\begin{aligned}\overline{p^2}_{\eta} + 2\alpha\overline{u^2}_{\eta} + 4\alpha^2\overline{w^2} - \mathrm{Ra}\;\overline{\theta^2} = {} & \frac{\overline{P^1}_{\eta}}{2} + \frac{\alpha\eta}{2}\overline{u^1}_{\eta\eta} + \alpha\overline{u^1}_{\eta} - \frac{3}{2}\alpha^3\eta\overline{u^1} \\ & - \frac{\mathrm{Ra}(1-\eta)}{2} \\ & + \mathrm{De}\; a\;\alpha(\alpha\overline{u^1}\overline{u^1}_{\eta} + \overline{w^1}\overline{u^1}_{\eta\eta}),\end{aligned} \tag{C5}$$

$$\begin{aligned}\overline{\theta^2}_{\eta\eta} + \overline{w^2} - 4\alpha^2\overline{\theta^2} = {} & \frac{\alpha\overline{u^1}}{2}(\overline{\theta^1} + \eta) + \frac{\overline{\theta^1}_{\eta}}{2}(\overline{w^1} - 3\alpha^2\eta) + \frac{\overline{w^1}}{2} + \overline{\theta^1}_{\eta\eta} \\ & - \frac{\alpha^2\eta}{2},\end{aligned} \tag{C6}$$

which is a set of nonhomogeneous ordinary differential equations. Note that q^2, r^2, and s^2 in Eqs. (32) and (33) have been expressed according to u^2 and w^2 [see Eqs. (35)–(38)]. The corresponding homogeneous boundary conditions are given by

$$\begin{pmatrix} \overline{u^2} \\ \overline{w^2} \\ \overline{\theta^2} \end{pmatrix}(\eta=0) = \begin{pmatrix} \overline{u^2} \\ \overline{w^2} \\ \overline{\theta^2} \end{pmatrix}(\eta=1) = \mathbf{0}. \tag{C7}$$

The system (C3)–(C6) with the boundary conditions above constitutes a boundary-value problem of the two-point type.

[1] L. J. Sobey, J. Fluid Mech. **96**, 1 (1980).
[2] D. J. Tritton, *Physical Fluid Dynamics*, 2nd ed. (Clarendon Press, Oxford, 1988)
[3] P. G. Drazin and W. H. Reid, *Hydrodynamic Stability* (Cambridge University Press, Cambridge, 1981).
[4] H. Zhou, R. J. Martinuzzi, R. E. Khayat, A. G. Straatman, and E. Aburamadan, Phys. Fluids **15**, 3114 (2003).
[5] R. Schmitz and W. Zimmerman, Phys. Rev. E **53**, 5993 (1996).
[6] R. Schmitz and W. Zimmerman, Phys. Rev. E **53**, R1321 (1996).
[7] K. Stork and U. Miller, J. Fluid Mech. **54**, 599 (1972).
[8] J. F. Thompson, Z. U. A. Warsi, and C. W. Mastin, *Numerical Grid Generation: Foundations and Applications* (North-Holland, New York, 1985).
[9] M. C. Cross, Phys. Rev. A **38**, 3593 (1988).
[10] L. Ning and R. E. Ecke, Phys. Rev. E **47**, R2991 (1993).
[11] Costas D. Dimitropoulos, Brian J. Edwards, Kyung-Sun Chae, and Anony N. Beris, J. Comput. Phys. **144**, 517 (1998).
[12] W. Zimmerman, M. Sesselberg, and F. Petruccione, Phys. Rev. E **48**, 2699 (1993).
[13] S. H. Davis, Annu. Rev. Fluid Mech. **8**, 57 (1976).
[14] R. E. Kelly and D. Pal, J. Fluid Mech. **86**, 433 (1978).
[15] M. N. Chen and J. A. Whitehead, J. Fluid Mech. **1**, 1 (1968).
[16] A. Watson and G. Poots, J. Fluid Mech. **49**, 33 (1971).
[17] H. Zhou, R. E. Khayat, R. J. Martinuzzi, and A. G. Straatman, Int. J. Numer. Methods Fluids **39**, 1139 (2002).
[18] S. Selvarajan, E. G. Tulapurkara, and V. Vasanta Ram, Phys. Fluids **11**, 579 (1999).
[19] J. Szumbarski and J. M. Floryan, J. Comput. Phys. **153**, 378 (1999).
[20] Z. Li and Roger E. Khayat, Phys. Rev. E (to be published).
[21] R. B. Bird, R. C. Armstrong, and O. Hassager, *Dynamics of Polymeric Liquids* (Wiley, New York, 1987), Vol. 1.